Improving Convenience and Reliability of 5-ALA-Induced Fluorescent Imaging for Brain Tumor Surgery

Hiroki Taniguchi[1], Noriko Kohira[1], Takashi Ohnishi[2], Hiroshi Kawahira[2]
Mikael von und zu Fraunberg[3], Juha E. Jääskeläinen[3], Markku Hauta-Kasari[4]
Yasuo Iwadate[5], and Hideaki Haneishi[2]

[1] Graduate School of Engineering, Chiba University, Chiba, Japan
[2] Center for Frontier Medical Engineering, Chiba University, Chiba, Japan
[3] Kuopio University Hospital, University of Eastern Finland
[4] School of Computing, University of Eastern Finland
[5] Graduate School of Medicine, Chiba University, Chiba, Japan
haneishi@faculty.chiba-u.jp

Abstract. This paper presents two features to make neurosurgery with 5-ALA-induced fluorescent imaging more convenient and more reliable. The first one is the concept for a system that switches between white light and excitation light rapidly and allows surgeons to easily locate the tumor region on the normal color image. The second one is the way for color signal processing that yields a stable fluorescent signal without depending on the lighting condition. We developed a prototype system and confirmed that the color image display with the fluorescent region worked well for both the brain of a dead swine and the resected tumor of a human brain. We also performed an experiment with physical phantoms of fluorescent objects and confirmed that the calculated flurophore density-related values were stably obtained for several lighting conditions.

Keywords: neurosurgery, fluorescent imaging, 5-ALA, protoporphyrin, color signal processing, real time processing

1 Introduction

In neurosurgery, fluorescence-based tumor region identification using 5-aminolevulinic acid (5-ALA) is being performed nowadays [1-5]. Within several hours after oral administration of 5-ALA prior to surgery, protoporphyrin IX (PpIX) is induced and it stays predominantly in malignant glioma cells. PpIX is a fluorophore which emits reddish fluorescence with the peak wavelength at 635 nm when it is excited by blue light. While the color of such malignant glioma cells looks similar to that of normal brain tissues under a white light, it is markedly different from the normal tissues under the excitation light.

So lately two kinds of light sources, a normal white light source and an excitation light source, are embedded in commercial operation microscopes (OMs) so that surgeons can change the light according to the operative procedure. Namely, surgeons confirm the fluorescent region in the brain under the excitation light, then they switch to the normal white light and resect the glioma.

N. Navab et al. (Eds.): MICCAI 2015, Part III, LNCS 9351, pp. 209–217, 2015.
DOI: 10.1007/978-3-319-24574-4_25

While this 5-ALA-based neurosurgery results in better identification of glioma in the operating room (OR), there are still two major issues. The first one is that the switching operation between the types of illumination is troublesome. Moreover, the surgeons must memorize where the fluorescent region appears under the excitation light or they must record the image prior to the resection of the glioma under the white light.

The second issue is the lack of quantitativity in the fluorescent images. Ideally, the glioma cell density should be known from the fluorescent image. In fact, currently it is hard to relate the image intensity of the fluorescent image to the glioma cell density. Ando et al. conducted a quantitative evaluation study and reported the relationship between the fluorescent intensities of tumor tissue and its pathological images [6]. Although the report is very informative, further investigation is still needed for practical use. At least, the intensity distribution of fluorescence should be independent of the lighting and imaging geometry. This is the first step to realize the estimation of the glioma cell density.

In this paper, we first propose a system overcoming the first issue. We then formulate the fluorescence imaging and present a processing way to avoid the geometrical effect for quantitative imaging. We then show some experimental results to confirm the performance of the proposed imaging system and the effectiveness of the color signal processing.

2 Concept of the Image Acquisition System

We assume that the OM has two kinds of light sources embedded, excitation light and normal white light, and also a color camera, an image processing unit (IPU) and a display device. Since the fluorescence takes place in the visible range, a conventional color camera can be used. The surgeon does not see the eye lens of the OM, but directly see the display attached on it. There is rapid switching between the two kinds of light sources. The frequency of the switching is typically 30 Hz. The color camera captures the image of the brain under each illumination synchronously. Roughly speaking, each image is captured in 1/60s. Although the surgical field has some flicker due to switching the light sources, it does not cause significant discomfort. Furthermore, by reducing the rate of the excitation light, it may be possible to make this less perceivable.

Obtained images are processed by IPU and displayed in real time. A pair of consecutive two frame images under different lights are processed and the resultant images are displayed. There are some ways to show the images. The simplest way is just to show the two images side by side on a display. In this paper, we implemented another display approach. After capturing the fluorescent image, the fluorescent region is segmented in 1/60s. Such segmented fluorescent regions are overlaid on the normal color image and displayed next to the normal color image. The real time image processing such as the segmentation and image display is computationally possible. Such a system makes the surgical workflow smoother.

As mentioned earlier, a stable processing for the fluorescent images is required for reliable use in OR. In this paper, color image processing to avoid the dependency on the lighting condition is mainly discussed as the first step of quantification.

3 Imaging Formula

Here we formulate the imaging of the object under the excitation light and show how to extract the contribution of the fluorescence. In this formulation, we introduced two assumptions. The first is that the bandwidth of spectral intensity of the excitation light is narrow enough so that the reflectance of the object can be approximated by a certain constant over the bandwidth. The second is that the spectral characteristics of the fluorescence do not change during the experiment. The second assumption should be checked carefully [7]. But to the extent of our experiment, the characteristics stay the same during at least one hour.

Prior to the formulation, we first define some parameters and functions as showing a schematic illustration and some graphs of spectral characteristics in Fig. 1.

$\mathbf{p}$: Position vector of a pixel in an image

$\mathbf{p}_o$: Position vector of the point in the surgical field corresponding to $\mathbf{p}$

$r(\mathbf{p}_o, \lambda)$: Spectral reflectance at $\mathbf{p}_o$

$E(\mathbf{p}_o, \lambda) = G(\mathbf{p}_o)e(\lambda)$: Spectral intensity of excitation light at $\mathbf{p}_o$

$G(\mathbf{p}_o)$: Geometry factor affecting spectral intensity. It includes distance between the light source and the object, normal direction of the object surface, etc.

$e(\lambda)$: Relative spectral characteristics of the excitation light (see Fig. 1(b) left)

$f(\lambda)$: Relative spectral characteristics of the fluorescence (see Fig. 1(b) right)

$h(\mathbf{p}_o)$: Fluorescence-related factor which implicitly includes density of the tumor cell, quantum efficiency, absorbance of the excitation light, etc.

$S_R(\lambda), S_G(\lambda), S_B(\lambda)$: Spectral sensitivities of red, green, blue channels of the color camera, respectively (see Fig. 1(c))

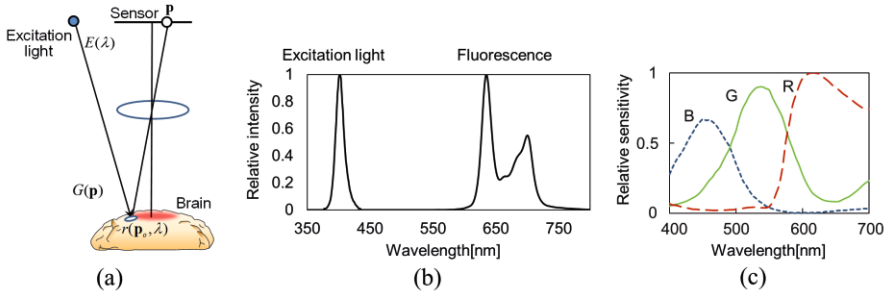

Fig. 1. Schematic illustration of lighting and imaging geometry (a), and relative spectral intensity of the fluorescence of PpIX (b) and spectral sensitivities of RGB camera (c).

Pixel value of the red channel at **p** in the image is then approximately modeled by,

$$g_R(\mathbf{p}) = \int [G(\mathbf{p}_o)e(\lambda)r(\mathbf{p}_o, \lambda) + G(\mathbf{p}_o)h(\mathbf{p}_o)f(\lambda)]s_R(\lambda)d\lambda \,. \quad (1)$$

In this model we assumed the diffuse reflection called Lambertian model. If we take into account the reflection and fluorescent phenomena more exactly, the above equation must be revised. Details will be discussed in the later section.

In Eq. (1), since we assume that the spectral band of the excitation light is narrow enough, the first integral of Eq. (1) is modified and Eq. (1) is expressed as

$$g_R(\mathbf{p}) = G(\mathbf{p}_o) r(\mathbf{p}_o, \lambda_0) \int e(\lambda) s_R(\lambda) d\lambda + G(\mathbf{p}_o) h(\mathbf{p}_o) \int f(\lambda) s_R(\lambda) d\lambda . \tag{2}$$

Here, $\lambda = \lambda_0$ represents the central wavelength of the narrow spectral band. Pixel values of green and blue channels $g_G(\mathbf{p})$ and $g_B(\mathbf{p})$ are given similarly by replacing the sensitivity function $s_R(\lambda)$ by $s_G(\lambda)$ and $s_B(\lambda)$, respectively.

These equations can be represented by a matrix form as

$$\begin{bmatrix} g_R(\mathbf{p}) \\ g_G(\mathbf{p}) \\ g_B(\mathbf{p}) \end{bmatrix} = \begin{bmatrix} a_{eR} & a_{fR} \\ a_{eG} & a_{fG} \\ a_{eB} & a_{fB} \end{bmatrix} \begin{bmatrix} G(\mathbf{p}_o) r(\mathbf{p}_o, \lambda_0) \\ G(\mathbf{p}_o) h(\mathbf{p}_o) \end{bmatrix} = \begin{bmatrix} \mathbf{a}_e & \mathbf{a}_f \end{bmatrix} \begin{bmatrix} G(\mathbf{p}_o) r(\mathbf{p}_o, \lambda_0) \\ G(\mathbf{p}_o) h(\mathbf{p}_o) \end{bmatrix} . \tag{3}$$

Here,

$$a_{ej} = \int e(\lambda) s_j(\lambda) d\lambda, \quad a_{fj} = \int f(\lambda) s_j(\lambda) d\lambda, \quad j = R, G, B$$

The right hand side of equation (3) is a combination of two vectors.

$$\begin{bmatrix} a_{eR} & a_{fR} \\ a_{eG} & a_{fG} \\ a_{eB} & a_{fB} \end{bmatrix} \begin{bmatrix} G(\mathbf{p}_o) r(\mathbf{p}_o, \lambda_0) \\ G(\mathbf{p}_o) h(v) \end{bmatrix} = G(\mathbf{p}_o) r(\mathbf{p}_o, \lambda_0) \mathbf{a}_e + G(\mathbf{p}_o) h(\mathbf{p}_o) \mathbf{a}_f \tag{4}$$

Two vectors can be obtained as follows. The RGB vector of the excitation light $\mathbf{a}_e$ is obtained by capturing the excitation light directly or through the reflection from a perfect reflecting diffuser (no fluorescence). On the other hand, the fluorescent light $\mathbf{a}_f$ can be obtained by capturing the PpIX solution illuminated by excitation light in a manner that the excitation light does not enter the camera. Then, from the RGB pixel values, two factors, $G(\mathbf{p}_o) r(\mathbf{p}_o, \lambda_0)$ and $G(\mathbf{p}_o) h(\mathbf{p}_o)$, can be determined using a least square method.

Next, we calculate the ratio of these two factors and define it as

$$v(\mathbf{p}) \equiv \frac{G(\mathbf{p}_o) h(\mathbf{p}_o)}{G(\mathbf{p}_o) r(\mathbf{p}_o, \lambda_0)} = h(\mathbf{p}_o) / r(\mathbf{p}_o, \lambda_0) . \tag{5}$$

This value is now geometry-independent because the geometry factor $G(\mathbf{p}_o)$ is cancelled. The more important value is $h(\mathbf{p}_o)$. From (5), this value is represented as

$$h(\mathbf{p}_o) = v(\mathbf{p}_o) r(\mathbf{p}_o, \lambda_0) . \tag{6}$$

This means that we need to know the reflectance distribution, $r(\mathbf{p}_o, \lambda_0)$. In fact, it is not easy to obtain $r(\mathbf{p}_o, \lambda_0)$. However, we suppose that the following procedure can provide a good estimation. A perfect reflecting diffuser is illuminated by the excitation light of the OM and its reflected intensity is captured by the color camera of the OM. This is done for many possible distances between the OM and the surgical field prior to the surgery. Intraoperatively, the reflection from the surgical field under the excitation light is recorded by the color camera. The blue channel values are divided by that of the perfect reflecting diffuser obtained at the same distance. These values should give approximately the reflectance $r(\mathbf{p}_o, \lambda_0)$.

4 Experiment

4.1 Prototype System Building

We built an experimental apparatus as shown in Fig. 2(a). It was composed of a white LED (IHRGB-120, IMAC co.), a high intensity blue LED with a peak at 405 nm (LEDH60-405, Hamamatsu Photonics), a CameraLink format color CCD camera (CLB-B1310C-SC, IMPERX), a frame grabber board (PIXCI-E4, EPIX), a hand-made switching circuit and a personal computer for controlling the illumination and image capture. Illumination switching is controlled by the strobe signal from the camera. The switching rate of the illumination was set to 30 Hz. The detailed timing chart of the operation is shown in Fig. 2(b).

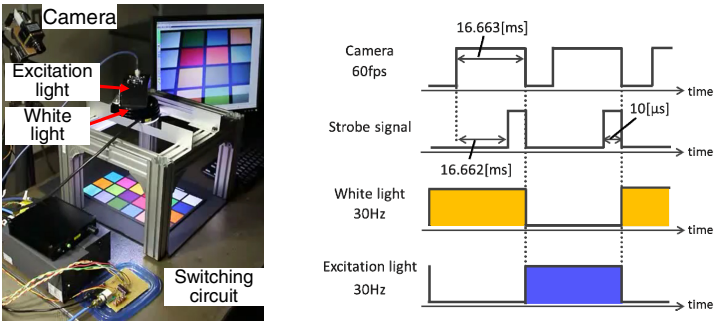

(a) Imaging system (b) Timing chart

Fig. 2. Lighting and imaging system (a) and the timing chart of operation (b).

4.2 Real Time Image Processing and Display

To confirm the performance of the system, a preliminary experiment with the brain of a dead swine was performed. PpIX solution was first made by dissolving PpIX powder (Sigma-Aldrich) with dimethyl sulfoxide. The density of the solution was 25mg/L. A small piece resected from the brain was soaked in the PpIX solution and then put on a fissure of the brain. An operator removed the piece from the brain as its operation was being captured and monitored by the system. Figs. 3 (a) and (b) show the image under the white light and the excitation light, respectively. Here the piece

with PpIX was located in the rightmost region in the images. It appeared as slightly reddish in Fig. 3(b).

In the image processing, the image under the excitation light was processed based on the formulas in section 3 to yield $v(\mathbf{p})$ given by Eq. (5). In order to segment the fluorescent region, some pre-processing and a thresholding operation were needed. As pre-processing, the saturated region (halation region) and a very dark region were removed. Then the fluorescent region was extracted by thresholding the $v(\mathbf{p})$ values. The parameters for those processings were determined empirically. Fig. 3(c) shows the segmented PpIX region overlaid on the image under the white light.

We then applied the prototype system to a real human glioma as well. Image acquisition was performed to a resected specimen from the glioma. A resected piece with about 2 cm length was put on a dish and the images were processed as before. Fig. 3 (d)-(f) show the results. We confirmed that the system worked for the resected specimen of a real human glioma as well.

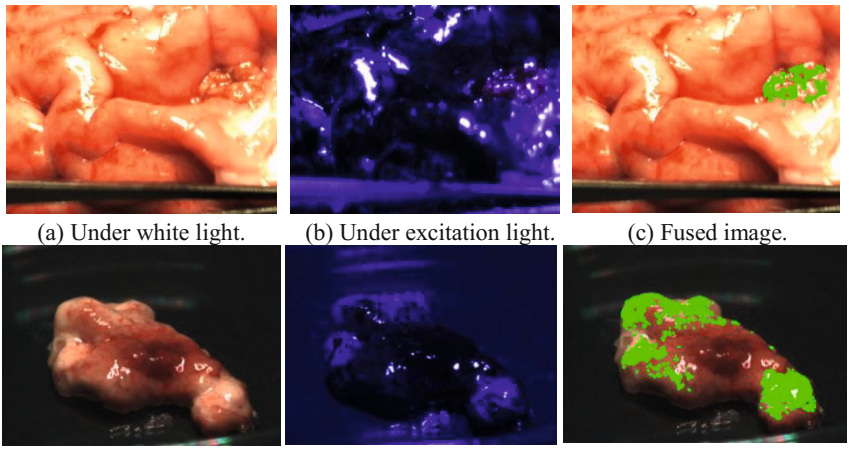

(a) Under white light. (b) Under excitation light. (c) Fused image.

(d) Under white light. (e) Under excitation light. (f) Fused image.

Fig. 3. Captured images in the experiment. (a)-(c): Swine brain. (d)-(f) Resected human glioma.

4.3 Quantitative Imaging Technique

We demonstrated the quantitative imaging technique shown in section 3. We showed that the intensity of the fluorescent image does not depend on the geometry. As shown in Eq. (6), the cell-related value $h(\mathbf{p}_o)$ does not depend on the geometry factor. We examined this formula using physical phantoms. First we measured the relationship between the PpIX density, d, and the h value at a certain lighting condition. That relationship was empirically modeled by an exponential function. Then the model was applied to the other measured images under the different lighting conditions.

In the experiment, PpIX solutions of seven different densities were made and then fixed with agar. The densities of the seven PpIX phantoms were

$$d = kC, \quad \text{where } k = 1,...,7,\ C = 3.0\times10^{-6}\,\text{mol/L}. \tag{7}$$

Fig. 4(a) shows a photo of the PpIX phantoms. Images of each phantom were captured under three different intensities and four different angles of light. As seen in Fig. 4(a), as the density increased, the color became dark. In the images $v(\mathbf{p})$ of these spatially uniform phantoms, a 10x10 pixels area was selected and the mean pixel values of the area $\bar{v}$ were calculated. On the other hand, the corresponding mean reflectance $\bar{r}$ was measured by a spectrophotometer. Fig. 4(b) shows the relationship between the density of the PpIX phantoms and h value in the case that the excitation light intensity was the highest and the illumination angle was 0 deg. Then the density of the PpIX was modeled by the following formula.

$$h(d) = \bar{v}(d)\bar{r}(d) = \alpha \exp(\beta d) \tag{8}$$

We determined two parameters α and β from the data under the highest intensity of the light. Then using the model, we estimated the densities of the phantoms from the images under the different lighting conditions.

Fig. 4(c) shows the results of the density estimation. Circles in the graph represent the mean values of estimated density among three different intensities of excitation light. The top and bottom of the error bars represent the maximum and minimum values of the estimated density, respectively.

Next the lighting angle independency was tested. The phantom of 3C was used and the lighting angle was changed as 15, 30, 45 and 60 deg from the normal direction. The mean, maximum and minimum estimated densities were 2.66C, 2.83C and 2.40C, respectively. In both two examinations, we achieved stable density estimation.

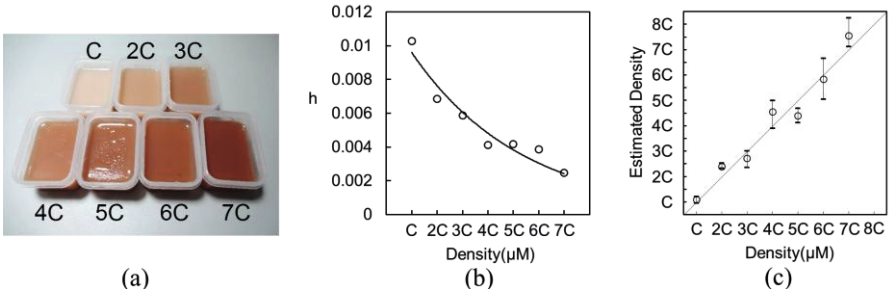

Fig. 4. Experiment for confirming the lighting condition-independent characteristics. (a) PpIX phantoms used. (b) Fitting curve. (c) Estimation result under different light intensities.

5 Discussion and Conclusions

With respect to real time image acquisition under two kinds of light sources, a similar approach was done by Sexton et al [8]. They used pulsed-light for excitation in addition to use of continuous white light. Their system requires an intensified CCD camera to achieve a very short time image acquisition. They did not refer to quantitative analysis. There are respectable works to quantify the fluorescence using fiber optics

[9] or multispectral camera [10]. The former technique measured point-by-point rather than 2D image. Although the latter can get 2D images, the system is bulky and real time processing is not possible. Our approach is a challenge to realize a both convenient and reliable system.

In section 2, we formulated both the value $v(\mathbf{p}_o)$ after cancellation of geometrical factor and the tumor cell density-related function $h(\mathbf{p}_o)$. In the first experiment, we focused on a real time processing and demonstrated the segmentation based on the value of $v(\mathbf{p}_o)$. On the other hand, in the second experiment, $v(\mathbf{p}_o)$ were related to $h(\mathbf{p}_o)$. In the next step, we must establish the real time estimation of $r(\mathbf{p}_o, \lambda_0)$ to get $h(\mathbf{p}_o)$.

In the quantification, we used the Lambertian model for the reflection and assumed that the geometrical factors for the reflection and fluorescence were the same. To be exact, however, more realistic model such as Phong model [11] consisting of the surface reflection and body reflection components. For example, direct reflection of the organ surface like mirror takes place in some parts. In such cases, a different image processing is required.

In this study, we proposed a method for real time image display with tumor location and built an experimental apparatus to confirm the performance. The apparatus was applied to a dead swine brain first then to a resected human brain tumor in OR. A neurosurgeon gave us a positive evaluation of this system. As future works, we need to clarify what is the appropriate switching rate, what are appropriate ways to carry out image processing and displaying. In the quantification of fluorescence, real mapping of the image values to the density of glioma cells is also needed.

Acknowledgments. This study is supported by MEXT/JSPS KAKENHI Grant Number 15H01106 in part.

References

1. Stummer, W., et al.: Intraoperative detection of malignant gliomas by 5-aminolevulinic acid-induced porphyrin fluorescence. Neurosurgery 42, 518–525 (1998)
2. Stummer, W., et al.: Fluorescence-guided surgery with 5-aminolevulinic acid for resection of malignant glioma: a randomised controlled multicentre phase III trial. Lancet Oncology 7(5), 392–401 (2006)
3. Widhalm, G., et al.: 5-Aminolevulinic acid induced fluorescence is a powerful intraoperative marker for precise histopathological grading of gliomas with non-significant contrast-enhancement. PLOS ONE 8(10), e76988 (2013)
4. Tonn, J.C., Stummer, W.: Fluorescence-guided resection of malignant gliomas using 5-aminolevulinic acid: practical use, risks, and pitfalls. Clinical Neurosurgery 55, 20–26 (2008)
5. Liao, H., et al.: An integrated diagnosis and therapeutic system using intraoperative 5-aminolevulinic-acid-induced fluorescence guided robotic Laser ablation for pre-cision neurosurgery. Medical Image Analysis 16(3), 754–766 (2012)
6. Ando, T., et al.: Precise comparison of protoporphyrin IX fluorescence spectra with pathological results for brain tumor tissue identification. Brain Tumor Path. 28, 43–51 (2011)
7. Ericson, M.B., et al.: A spectroscopic study of the photobleaching of protoporphyrin IX in solution. Lasers in Medical Science 18(1), 56–62 (2003)

8. Sexton, K., et al.: Pulsed-light imaging for fluorescence guided surgery under normal room lighting. Optics Letters 38(17), 3249 (2013)
9. Kim, A., et al.: Quantification of in vivo fluorescence decoupled from the effects of tissue optical properties using fiber-optic spectroscopy measurements. Journal of Biomedical Optics 15(6) (2010)
10. Valdés, P.A., et al.: Quantitative, spectrally-resolved intraoperative fluorescence imaging. Scientific Reports 2, Article number 798 (2012)
11. Phong, B.T.: Illumination for computer generated pictures. Communications of ACM 18(6), 311–317 (1975)